ORNL/SPR-2019/1355

Viability of Data Analytics to Ascertain Component Performance for Additive Manufacturing

L. Scime
J. Haley
V. Paquit

September 2019

M2CT-19OR06090136
TCR-DP-RPRT-002

OAK RIDGE NATIONAL LABORATORY
MANAGED BY UT-BATTELLE FOR THE US DEPARTMENT OF ENERGY

ORNL/SPR-2019/1355

Transformational Challenge Reactor

VIABILITY OF DATA ANALYTICS TO ASCERTAIN COMPONENT PERFORMANCE FOR ADDITIVE MANUFACTURING

L. Scime
J. Haley
V. Paquit

September 2019

M2CT-19OR06090136
TCR-DP-RPRT-002

Prepared by
OAK RIDGE NATIONAL LABORATORY
Oak Ridge, TN 37831-6283
managed by
UT-BATTELLE, LLC
for the
US DEPARTMENT OF ENERGY
under contract DE-AC05-00OR22725

CONTENTS

LIST OF FIGURES v
ABSTRACT 7
1. INTRODUCTION 7
2. AVAILABLE DATA STREAMS 7
2.1 In Situ Data Analytics Capabilities: Peregrine 8
2.1.1 Dynamic Segmentation Convolutional Neural Network 9
2.1.2 Remote Monitoring 12
2.1.3 On-Axis Data Streams 13
2.1.4 Ex Situ Correlations 14
2.2 In Situ Data Analytics Development: Scops 14
2.2.1 Laser Head and Nozzle Assembly Tracking and Working Distance Monitoring 14
2.2.2 Digital Image Correlation for 3D Mapping and Strain Calculation 15
3. CORRELATION OF IN SITU DATA WITH EX SITU OBSERVATIONS 16
3.1 Direct Detection of Defects 16
3.2 Classical Statistical Correlations 19
3.3 Unsupervised Machine Learning 19
3.4 Registration with White Light Scans 20
3.5 In Situ and Ex Situ Topological Accuracy with Structured-Light Scanning 21
3.6 Surface Roughness Correlation 22
4. CONCLUSION 23

LIST OF FIGURES

Figure 1: Laser powder-bed data: 7

Figure 2: Binder-jet data: 8

Figure 3: Directed-energy deposition data: 8

Figure 4: Representative examples of selected surface-visible anomalies detected by Peregrine. 9

Figure 5: The dynamic segmentation convolutional neural network classifications overlaid (as false colors) on a mid-wave infrared powder-bed image from an ExOne M-Flex system. 10

Figure 6: A "heat map" indicating the cumulative detections of *minor superelevation* throughout the height of the build for a Concept Laser M2 system. 10

Figure 7: A plot of the anomaly classifications as a function of build height for a Concept Laser M2 system. 11

Figure 8: A 3D reconstruction of a part printed on the ExOne M-Flex system based on dynamic segmentation convolutional neural network classifications. 11

Figure 9: The "Mission Control" portal allowing for remote monitoring of the builds. 12

Figure 10: Anomaly detections through the height of an ExOne M-Flex build for which the process parameters were autonomously adjusted by Peregrine. 12

Figure 11: Preliminary results from a thermal probe scan on the Concept Laser M2 machine. 13

Figure 12: Laser head tracking and processing in directed-energy deposition system. 15

Figure 13: Sample results for stereo digital image correlation (DIC). 16

Figure 14: Direct detection of defects. 17

Figure 15: Image taken after the completion of the build 17

Figure 16: Reconstruction of the dynamic segmentation convolutional neural network pixel classifications, in which the "witness line" is also visible. 18

Figure 17: In situ data showing shifts in the laser alignment (left) confirmation that the laser shift remains constant throughout the remainder of the build, (middle) the more pronounced shift toward the rear of the Concept Laser M2 machine, and (right) the less pronounced shift toward the front of the M2. 18

Figure 18: Dynamic segmentation convolutional neural network detections of *soot* and *debris* near a given sample component plotted against the programmed energy density of the sample component. 19

Figure 19: Clustering of samples from a process parameter study using t-distributed stochastic neighbor embedding. 20

Figure 20: Comparison of detection of defect in situ and the location of the failure point in the physical object. 21

Figure 21: Comparison of ex situ structured-light scanning (left) to in situ digital image correlation (right). 21

Figure 22: Comparison of in situ high resolution imaging system (left) and ex situ confocal microscopy measurements (right). 22

Figure 23: Infrared signal intensity variation due to surface roughness. 23

ABSTRACT

The Transformational Challenge Reactor (TCR) program is leveraging additive manufacturing (AM) technologies to produce multiple nuclear components to be assembled into a fully functional microreactor core. AM was selected as the main manufacturing technology for TCR because it has the potential to disrupt the nuclear industry on two fronts: (1) it enables the manufacturing of very complex geometries with optimized and tailored material properties for the intended use of the component, opening up new options for reactor designs, and (2) it allows for a better understanding of the manufacturing process through real-time in situ monitoring, data analytics, and artificial intelligence, which can lead to a streamlined qualification and certification process. Within TCR, the development and deployment of a digital platform aims at addressing the latter opportunity. As part of this effort, the collection of pedigree datasets is vital, should these data be generated before, during or after the manufacturing process.

This report focuses on the development of data analytics tools enabling qualitative assessment of the manufacturing processes to automate the identification of flaws in in situ monitoring imagery and to correlate those flaws to the resulting mechanical testing data. Through examples, the report gives an overview of the data collected and presents a path forward for the digital platform.

1. INTRODUCTION

This document provides details on the data analytics approach developed during the period of performance covered by this report. The document is structured as follows: a brief overview is provided of the various data modalities collected either in situ or ex situ. The report then describes the data analytics tools "Peregrine" and "Scops" used to process powder-bed system data and directed-energy deposition (DED) data, respectively. The findings are illustrated through examples and comparisons between in situ and ex situ data to show the viability of the approach.

2. AVAILABLE DATA STREAMS

Three main classes of 3D printers were used: laser powder bed, binder jet, and DED. Most of these systems are equipped with basic sensing functionalities recorded in log files. Additionally, some of them have been equipped with more advanced in situ monitoring cameras, either by the manufacturer or by the Transformational Challenge Reactor (TCR) program team. Figure 1 to 3 show examples of the image data we are working with.

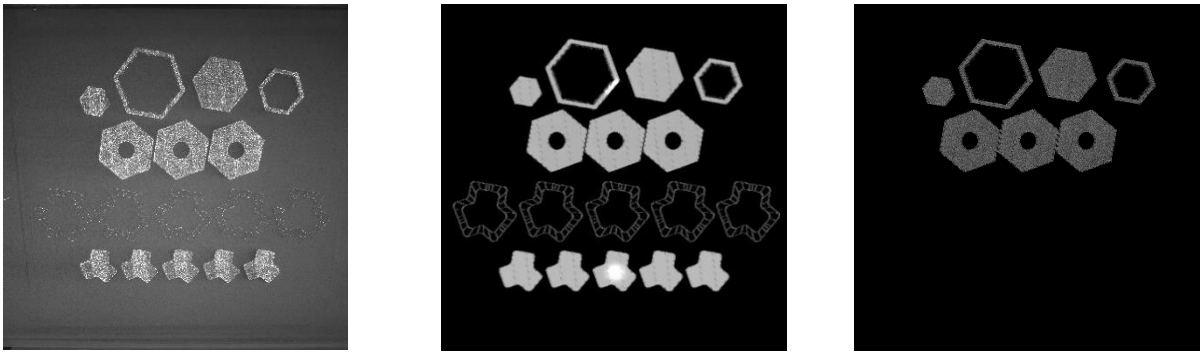

(a) **(b)** **(c)**

Figure 1: Laser powder-bed data: (a) visible-light powder-bed image, (b) spatially mapped on-axis photodiode data, and (c) spatially mapped on-axis camera data. Note that for all the builds to date, the on-axis camera for at least one of the two lasers has malfunctioned.

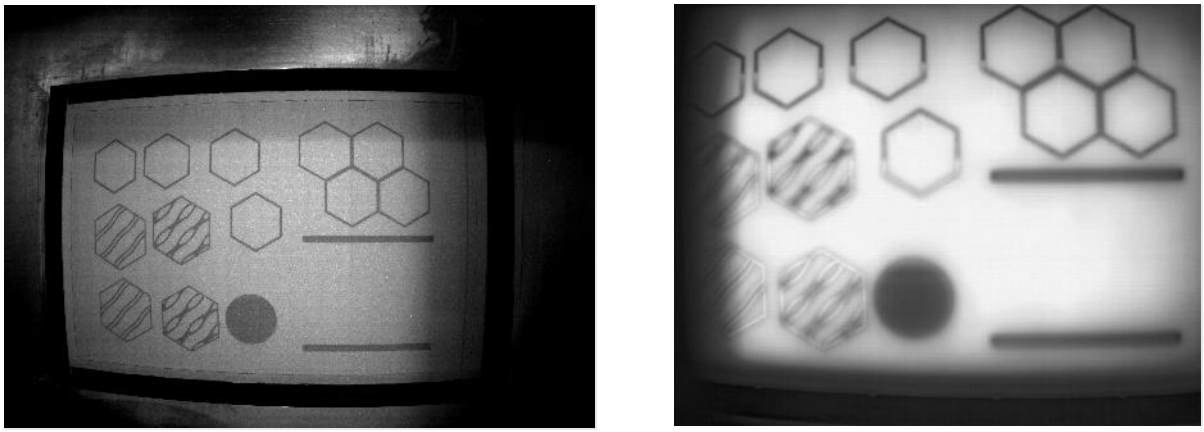

(a) **(b)**

Figure 2: Binder-jet data: (a) visible-light powder-bed image and (b) mid-wave infrared powder-bed image.

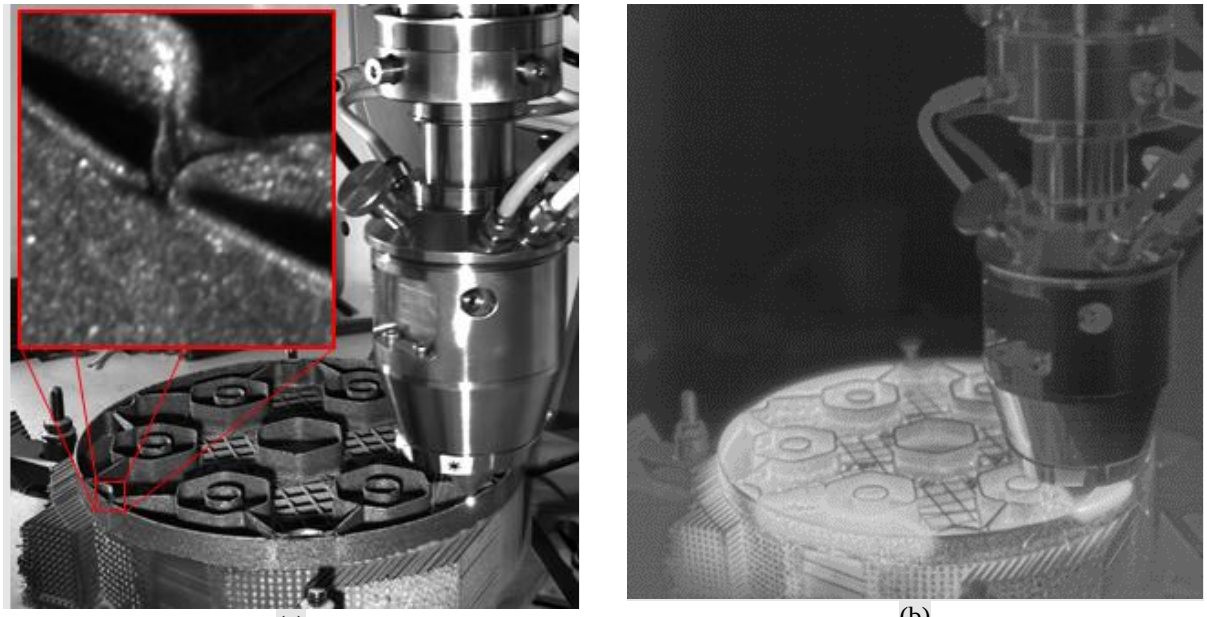

(a) (b)

Figure 3: Directed-energy deposition data: (a) off-axis 20 MP visible-light inspection camera and (b) off-axis FLIR Boson long wave infrared camera.

2.1 IN SITU DATA ANALYTICS CAPABILITIES: PEREGRINE

Peregrine is a software package developed by Oak Ridge National Laboratory (ORNL) to provide an end-to-end solution for in situ data collection, analysis, and visualization for powder-bed systems. Peregrine encompasses the following core capabilities.

1. Fusion and automated analysis of multiple sensor modalities using a purpose-designed machine learning (ML) model called a dynamic segmentation convolutional neural network (DSCNN).
2. Remote monitoring of the builds, allowing the machine operators to structure their schedules more efficiently.
3. Collecting metadata about each build from the machine operators
4. Parsing the machine-specific log files and plotting time-series data.

5. Spatial mapping of certain on-axis data streams.
6. Correlation of in situ data with ex situ observations.

Peregrine currently operates in local computing environments but will eventually be moved to a server to handle the large amount of data generated by the TCR program. For reference, the current data burden ranges from 1 MB/layer (FormUp 350) to 20 MB/layer (Innovent/Innovent^{+}) with individual builds generating up to 100 GB of data once they are decompressed for analysis and visualization. The capabilities of Peregrine continue to expand as more in situ sensor modalities come online and as needs develop for additional data analytics.

2.1.1 Dynamic Segmentation Convolutional Neural Network

The DSCNN can ingest any layer-wise data streams that are spatially correlated to make anomaly and defect classifications. For example, the DSCNN uses the post-binder and post-powder images from both the visible-light and mid-wave infrared cameras (a total of four images) when predicting anomalies on the M-Flex binder-jet system. For laser powder-bed systems the following classifications can be made about each pixel in the original images: *powder is okay*, *printed part is okay*, *recoater hopping*, *recoater streaking*, *incomplete spreading* (short feed), *debris*, *minor superelevation* (swelling), *major superelevation*, *soot* (spatter particles), and *misprints*. For binder-jet systems, the following classifications can be made about each pixel in the original images: *powder is okay*, *printed part is okay*, *recoater streaking*, *incomplete spreading* (short feed), *debris*, and *misprints*. Figure 4 summarizes these anomaly types.

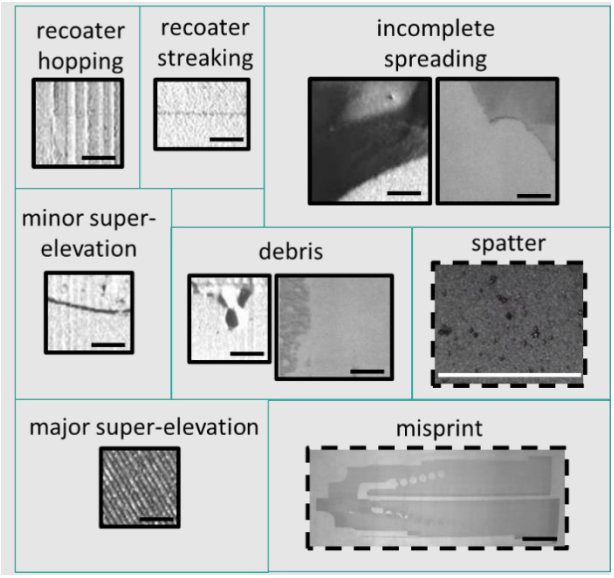

Figure 4: Representative examples of selected surface-visible anomalies detected by Peregrine. Solid borders denote images taken immediately after powder deposition, while dashed borders denote images taken immediately after powder-fusion or binder deposition. All scale bars are 10 mm in length.

The smallest defect detectable is limited by the camera resolution in combination with the camera's field of view; the effective pixel sizes are on the order of 100 µm for powder-bed systems. Also note that defect detection is also dependent upon the sensing modality, for example, subsurface defects such as many types of porosity are not detectable using visible-light imaging of the powder bed. Direct comparisons between the printed parts and the intended geometries can currently be made for all the powder-bed systems except the FormUp 350 and the X Line 2000R with a tolerance driven by the accuracy of the image registration scheme and any inter- or intrabuild variance in the imaging system or machine coordinates.

Once the layer-wise data are collected, analysis of each layer requires between 5 and 15 s per layer depending on the powder bed-process and the data modalities included. After analysis by the DSCNN, the pixel-wise classifications (i.e., anomaly detections) are viewed using multiple techniques including overlaying them on the raw data (Figure 5), generating heat maps of their cumulative occurrences throughout the build (Figure 6), plotting them as functions of build height (Figure 7), and displaying them as full 3D reconstructions (Figure 8).

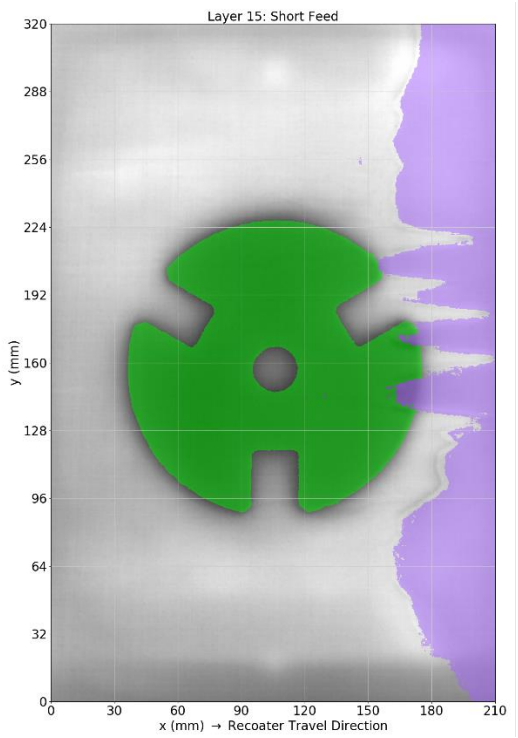

Figure 5: The dynamic segmentation convolutional neural network classifications overlaid (as false colors) on a mid-wave infrared powder-bed image from an ExOne M-Flex system.

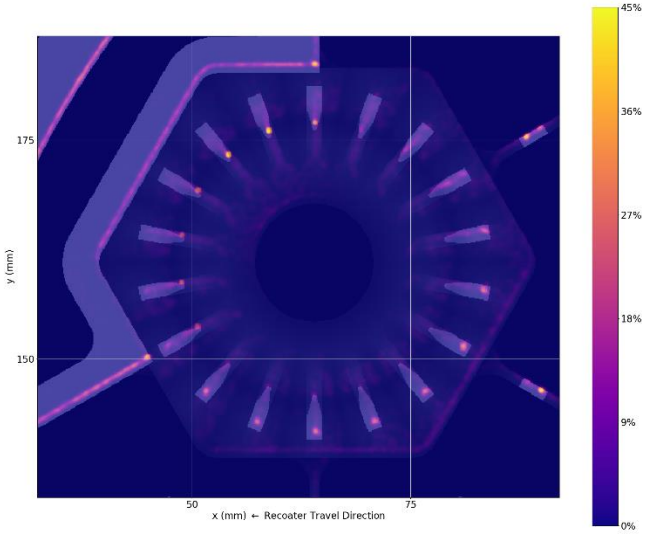

Figure 6: A “heat map” indicating the cumulative detections of *minor superelevation* throughout the height of the build for a Concept Laser M2 system.

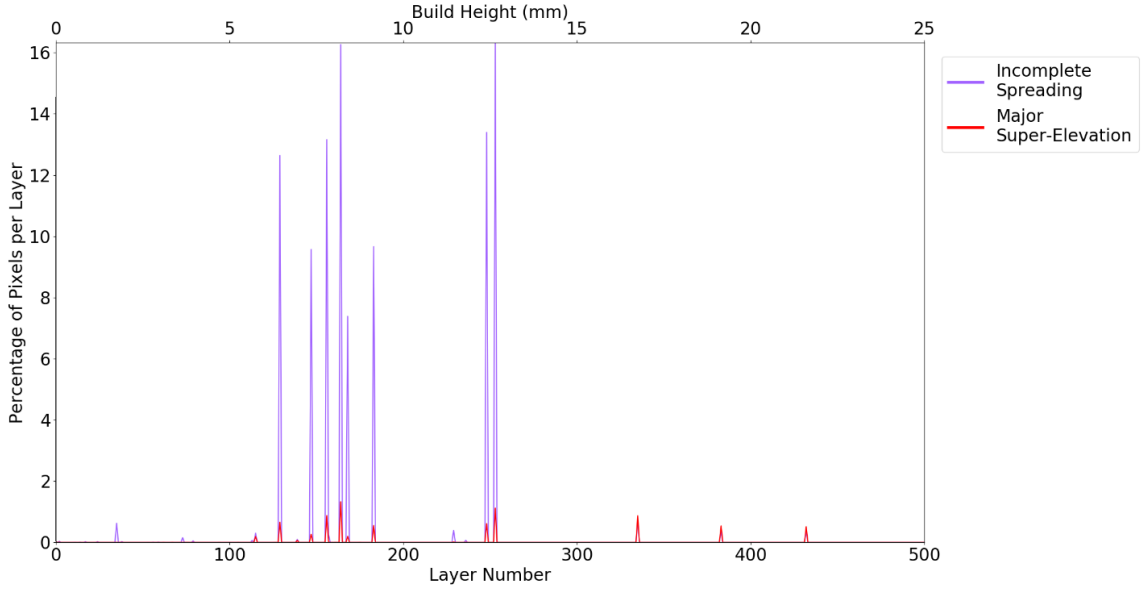

Figure 7: A plot of the anomaly classifications as a function of build height for a Concept Laser M2 system.

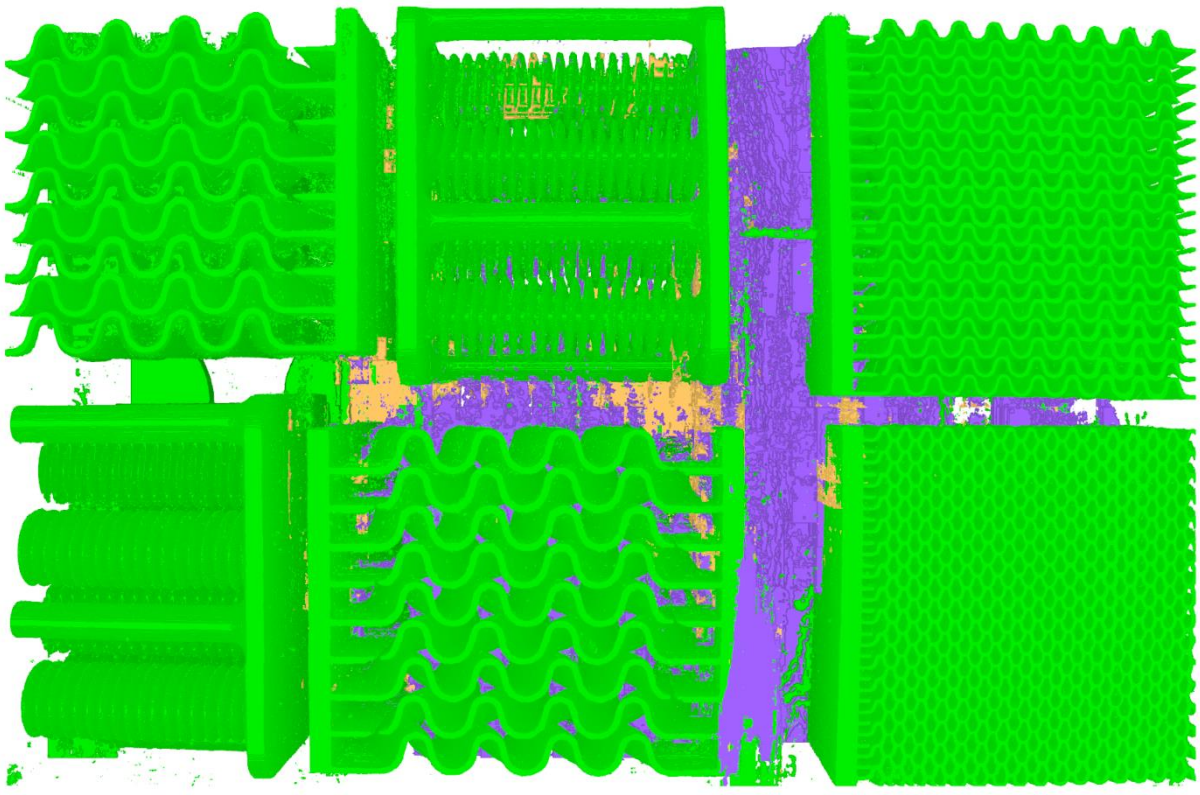

Figure 8: A 3D reconstruction of a part printed on the ExOne M-Flex system based on dynamic segmentation convolutional neural network classifications.

2.1.2 Remote Monitoring

Peregrine runs “live” (i.e., in real time) on all binder-jet machines used for the TCR program. This allows the machine operators to monitor the status of the prints remotely through automated email/text alerts as well as a portal (Figure 9) showing the current and previously printed layers with any detected defects highlighted. Rudimentary closed-loop process control has also been demonstrated for the ExOne M-Flex binder-jet machine. Figure 10 shows anomaly detections for an M-Flex build in which Peregrine identified that a short feed was occurring and autonomously adjusted the powder spreading process parameters to correct the issue.

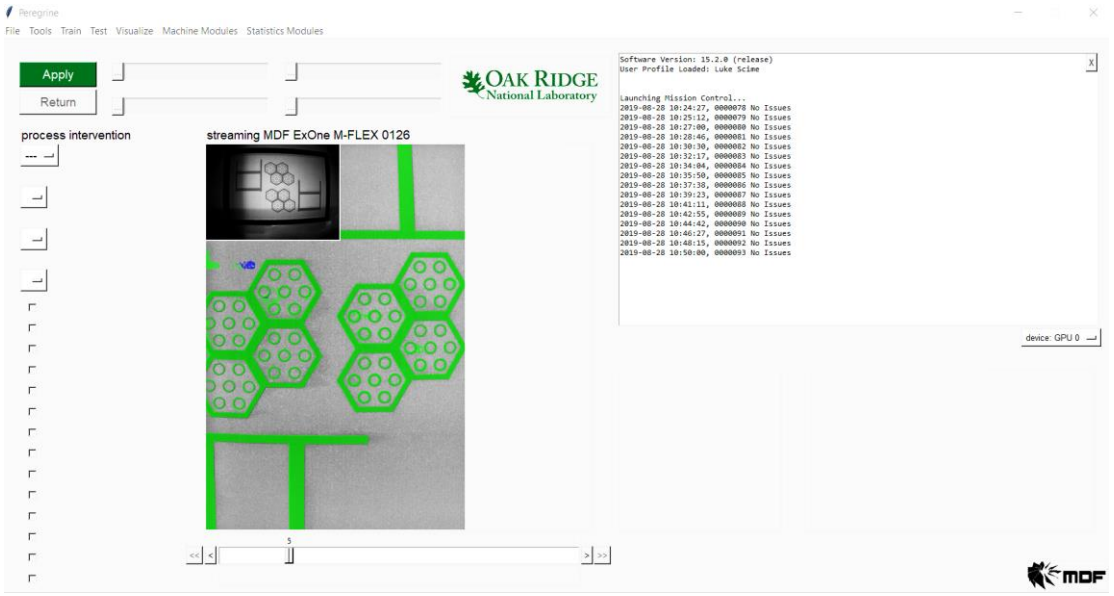

Figure 9: The “Mission Control” portal allowing for remote monitoring of the builds.

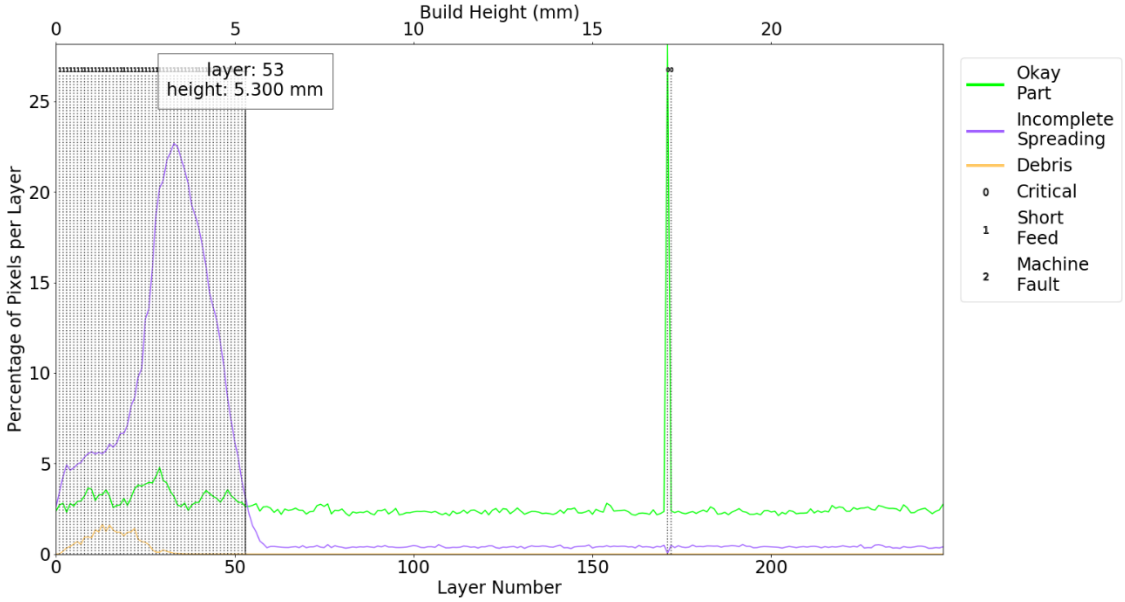

Figure 10: Anomaly detections through the height of an ExOne M-Flex build for which the process parameters were autonomously adjusted by Peregrine.

2.1.3 On-Axis Data Streams

Unique among the powder-bed machines used by the TCR program, the Concept Laser M2 produces on-axis data in addition to off-axis layer-wise data. Specifically, a camera and a photodiode are integrated into the laser optic train such that their fields of view follow the path of the melt pool during the build. These data, which are initially stored as time series, are spatially mapped into real space by Peregrine, as shown in Figure 11b and Figure 11c. Because of the spectral sensitivities of these sensors, the signal intensities are expected to be driven primarily by short-wavelength emissions from the vapor plume above the melt pool and may be influenced by retro-reflected laser light. As a result, while these signal intensities will be correlated with input energy levels, it is not expected that direct observation of flaws will be possible using these modalities. Work is ongoing to determine whether flaws may be detected indirectly through correlation of nonhuman interpretable features with ex situ analyses (e.g., x-ray computed tomography). Additionally, the TCR team has identified multiple problems with data collection and sensor robustness that must be addressed by the machine manufacturer.

Because of the challenges of using these on-axis sensors as intended by the machine manufacturer, a novel technique using the same/similar sensor hardware is being explored with the goal of enabling direct observation of subsurface defects such as lack-of-fusion porosity. This technique, called thermal probe scanning (TPS) uses one of the Concept Laser M2's lasers to "probe" a just-printed layer with a very low power beam. Because the thermal diffusivity of unmelted powder is substantially lower than that for the bulk material, the temperature field should be distinct when the scan passes over a region with a subsurface pore, and this difference should be observable by the on-axis photodiode. Figure 11 shows some preliminary results from TPS. Because of the spectral sensitivity of the current on-axis photodiode, the intensities are likely correlated with reflected laser light and not subsurface thermal fields; a photodiode with a longer wavelength response will be purchased to replace the Concept Laser–installed photodiode. Because the final output of the TPS is a spatially registered image, these data can be directly "fused" with the visible-light powder-bed images by Peregrine's DSCNN.

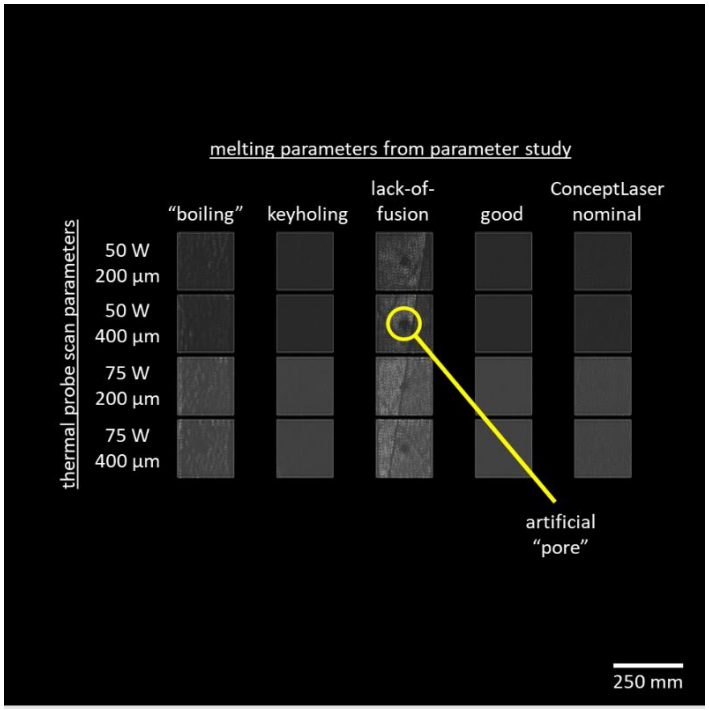

Figure 11: Preliminary results from a thermal probe scan on the Concept Laser M2 machine. Note that the artificial pore created for this experiment is surface connected.

2.1.4 Ex Situ Correlations

In its final implementation, the TCR digital thread will serve as a robust model linking "cheap" in situ data to materials performance and reactor part quality metrics. For example, direct or indirect porosity detections will be used to predict the fatigue/thermal cycling performance of a component within the reactor. A summary of the in situ to ex situ correlation efforts to date is provided in Sect. 3.

2.2 IN SITU DATA ANALYTICS DEVELOPMENT: SCOPS

In a five-axis DED system, the sides of the part remain exposed, which permits optical measurement of the entire outer skin of the part—unlike in a powder-bed system, which can only monitor the top of the most recent layer. This enables a higher dimensionality of information to be collected from a build; each outer surface can be tracked through time. This requires a differently structured data analytics scheme capable of applying spatial transformations to image sets to overlay acquired information onto the geometry of the part. In keeping with the more mature "Peregrine" software, the "Scops" hardware-software package is under active development to effect the following in DED systems.

1. Automated collection, 3D reconstruction, analysis, and storage of multimodal measurements
2. Remote monitoring of builds to assist the machine operator.
3. Synthesis of off-axis measurements with on-axis and time logged data for spatially localized multidimensional characterization.
4. Automated event-based triggering of higher time-resolution data collection to better capture unusual artifacts
5. Enabling the correlation of in situ data with ex situ observations.

Currently, Scops is capable of recording, organizing, and providing remote monitoring for operators, which has provided the datasets for manual analyses discussed in the following sections.

2.2.1 Laser Head and Nozzle Assembly Tracking and Working Distance Monitoring

In sprayed powder DED, a critical process parameter is working distance—the gap between the end of the powder spray nozzle and the melt pool. The relative position of the two determines how well focused both the laser and the powder stream are, which can alter the mass capture efficiency and effective input power. One capability currently being developed is to extract the position of the nozzle and the melt pool and calculate the working distance in real time at up to 18 Hz using the off-axis stereo high-resolution cameras installed with Scops. In Figure 12(a), the raw image shows a tracking marker (sun) used to rapidly identify head coordinates using stereo vision. In Figure 12(b), the prior image is subtracted from it, removing background to clearly show the powder spray pattern below the nozzle. The tracking marker (sun) is visible during the print, from which the position can be extracted, and other information can be found using various filtering techniques.

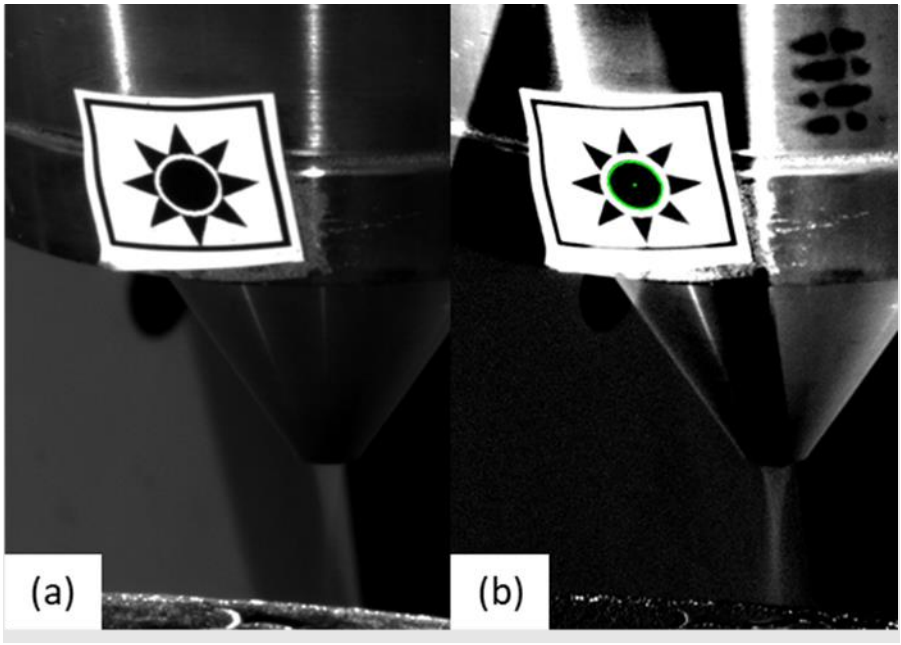

Figure 12: Laser head tracking and processing in directed-energy deposition system. In (a), the raw image shows a tracking marker (sun) used to rapidly identify head coordinates using stereo vision. In (b), the prior image is subtracted from it, removing the background to clearly show the powder spray pattern below the nozzle.

2.2.2 Digital Image Correlation for 3D Mapping and Strain Calculation

One of the core technical requirements of Scops is the ability to take an off-axis image and map it onto the 3D geometry for registration between sets of measurement signals. To produce a 3D measurement of the surface, the established technique of stereo digital image correlation (DIC) is used. DIC functions by carefully measuring the lens distortions and transformation between two cameras, taking an image of the part, and then matching textured image subsets from one camera to the next to triangulate the position of the surface. The results of the DIC process are highlighted in Figure 13a and Figure 13b. In addition to mapping, DIC can track the same features over time, providing a local measurement of displacement and strain history. This was demonstrated to resolve strains as low as 0.2% under manual compression in Figure 13c.

While DIC typically has stringent requirements on the optical appearance of a diffuse, correlatable pattern on the target surface, it was discovered through preliminary experiments that the surface roughness in DED produced by welded-on powder particles provided an excellent correlation pattern. This permits true in situ measurement of the 3D surface and strains.

The requirement of using the natural surface roughness of the part for correlation imposes optical and hardware limitations, as the roughness must be resolved at a sufficiently high resolution. Through further optical experimentation it was found that a projected pixel size of 80 µm was the upper limit, meaning that for successful correlation over large build volumes of 300–400 mm a set of high-resolution cameras was required. Additionally, the angles of illumination are critical as shifting light produces a change in the specular highlight on a particle and its apparent position. Resolving these and other issues allows for a data substrate 3D profile onto which such information as infrared temperature measurement, surface roughness, and other optically measurable parameters can be mapped.

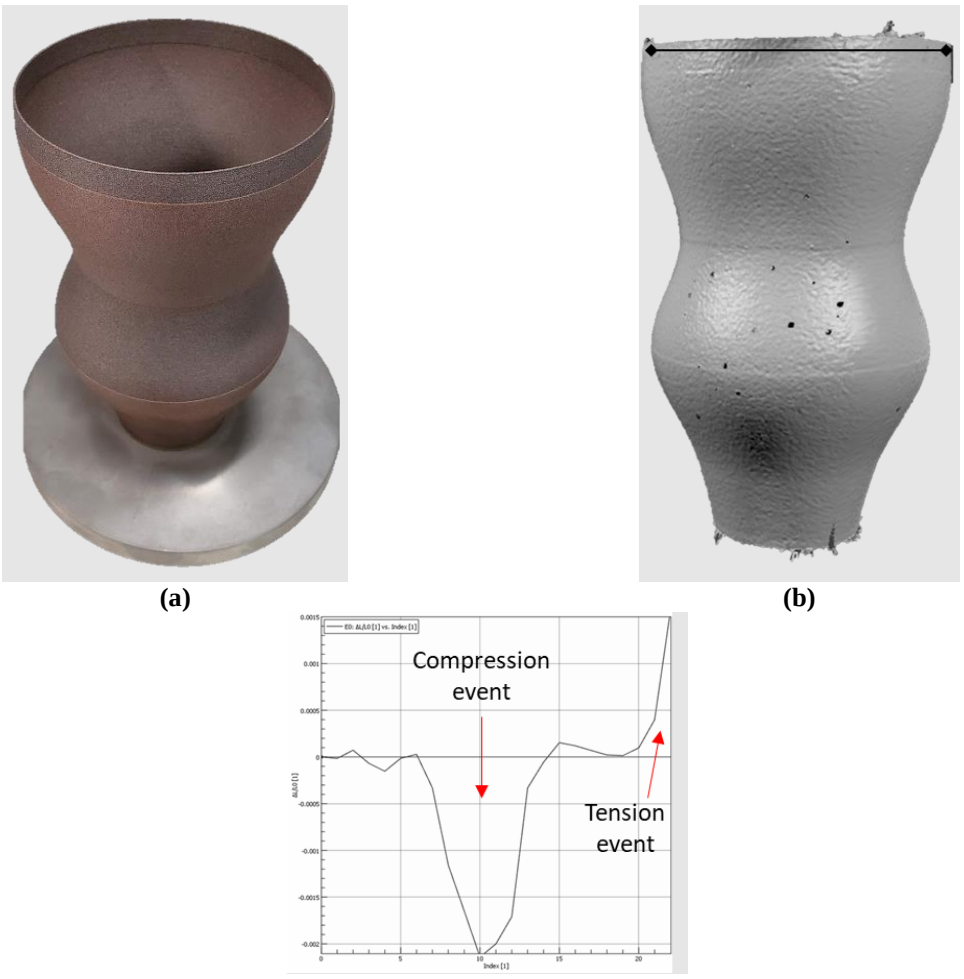

Figure 13: Sample results for stereo digital image correlation (DIC). A DED fabricated component shown in (a) was measured with DIC to provide accurate 3D scan (b). This scan uses existing surface roughness for correlation features. The virtual DIC strain gauge labelled in black in (b) was measured while manually squeezing the component, and strain is plotted in (c). demonstrating strain detection limits better than 0.2%

3. CORRELATION OF IN SITU DATA WITH EX SITU OBSERVATIONS

If a defect can be identified in the in situ data with the human eye, direct detection of the flaw is possible. Alternatively, the in situ data may contain the information needed to detect a flaw, but the salient features may not be "human interpretable." Such a situation necessitates indirect detection for which additional ex situ data (e.g., an x-ray computed tomography reconstruction) is used to identify the salient features and train an ML model to detect the anomalies using only the in situ data.

3.1 DIRECT DETECTION OF DEFECTS

Misprints on the Concept Laser M2 machine are directly detectable flaws. During a *misprint*, material is fused in a location not specified by the part designers nor indicated by the 3D model of the part. A direct comparison between the DSCNN's fused powder detections and the registered CAD information makes such a flaw highly evident, as shown in Figure 14.

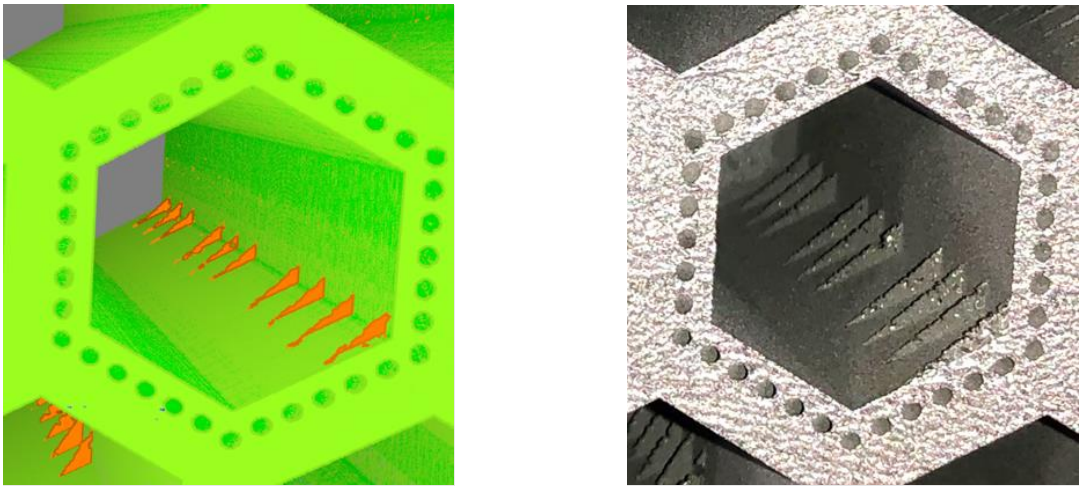

(a) **(b)**

Figure 14: Direct detection of defects. *Misprints* are highlighted in orange by the dynamic segmentation convolutional neural network in (a) and are visible ex situ on the as-built part in (b).

Shifts in the laser alignment on the Concept Laser M2 are also directly detectable. Laser shifts may occur when a build is paused and restarted, as occurred for the tubes shown in Figure 15 after about 50 mm of build height. This "witness line" is eminently visible ex situ and can also be observed in the reconstruction of the in situ data (Figure 16).

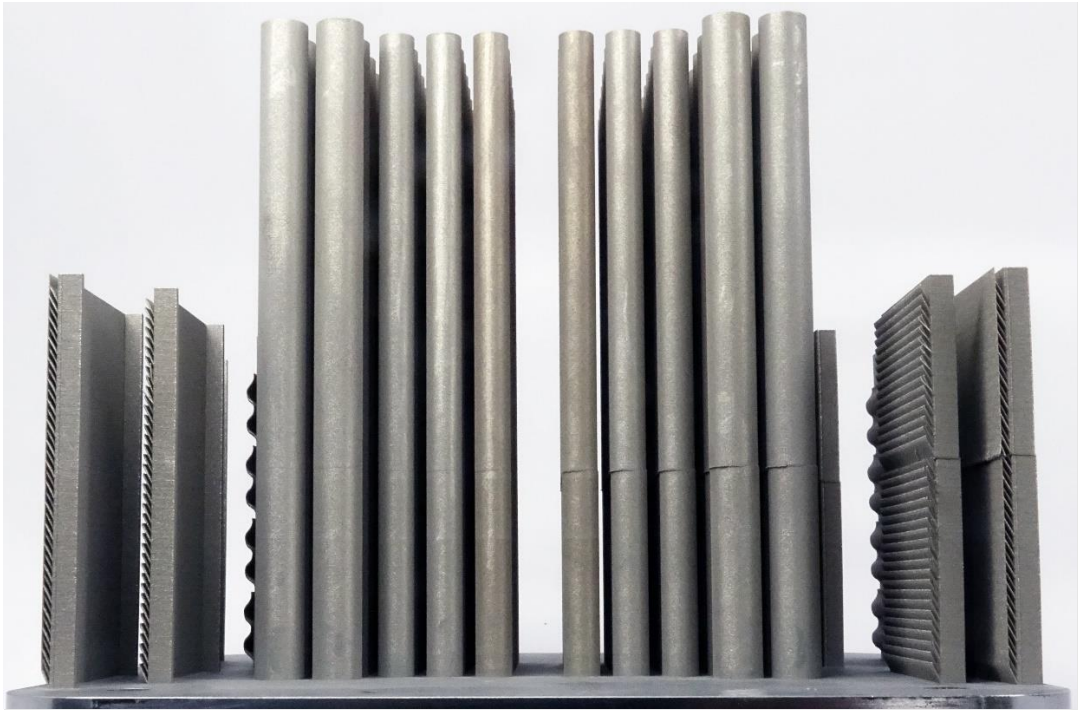

Figure 15: Image taken after the completion of the build; observe the "witness line" located about one third up the height of the build.

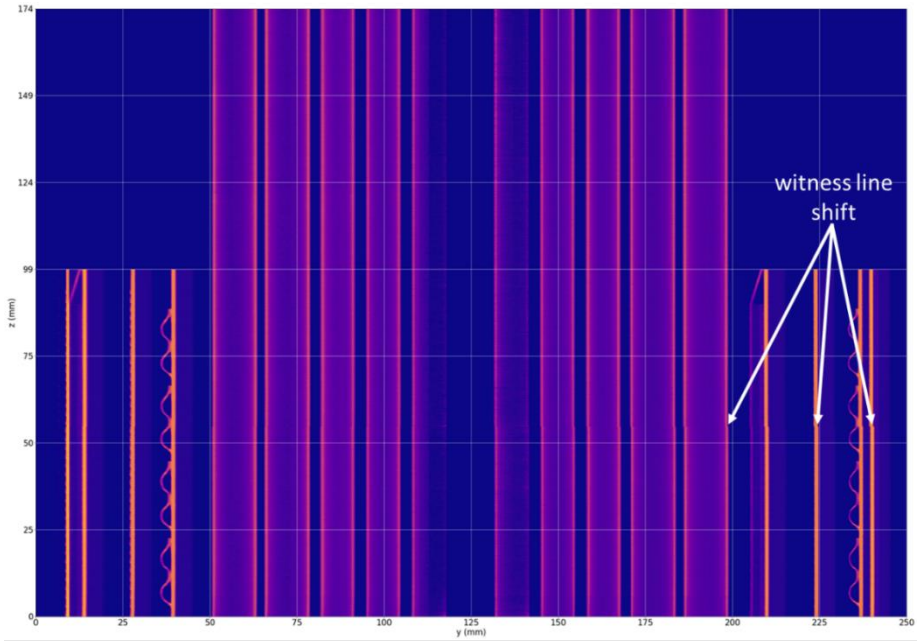

Figure 16: Reconstruction of the dynamic segmentation convolutional neural network pixel classifications, in which the "witness line" is also visible.

Closer inspection of the in situ data (Figure 17) reveals that the laser shift is substantially more pronounced toward the rear of the M2 (laser module 1) than toward the front of the M2 (laser module 2). This contrast is also visually apparent ex situ, where the front and rear of the M2 are left and right, respectively, in Figure 15. Based on the in situ data, the magnitude of the shift is about 500 µm in the rear and less than 100 µm in the front. It is also apparent that the shift is permanent; that is, for the remainder of the build the lasers remain offset from their positioning at the beginning of the build.

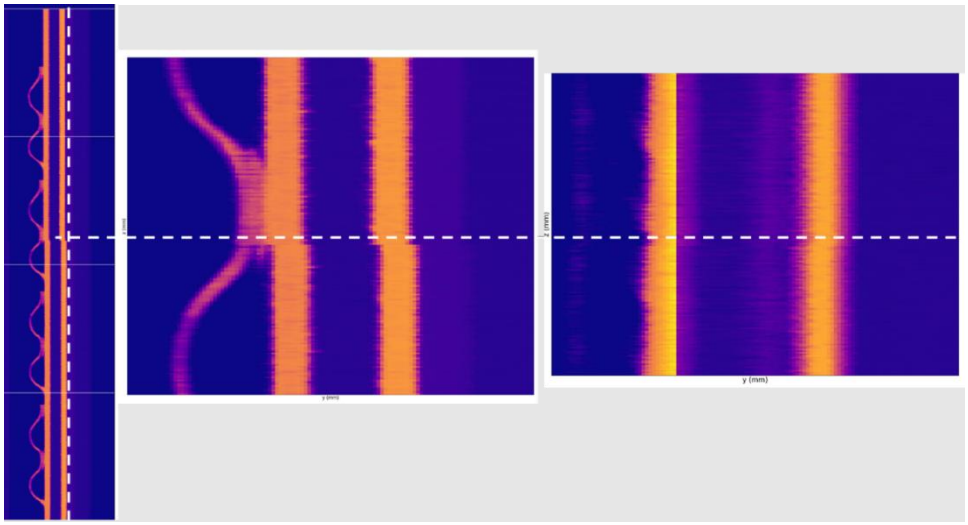

Figure 17: In situ data showing shifts in the laser alignment (left) confirmation that the laser shift remains constant throughout the remainder of the build, (middle) the more pronounced shift toward the rear of the Concept Laser M2 machine, and (right) the less pronounced shift toward the front of the M2.

3.2 CLASSICAL STATISTICAL CORRELATIONS

Flaws detected using classical statistical correlations should be considered to lie between *direct* and *indirect* detections as they may still be human interpretable but cannot be directly observed in the in situ data. A common technique known as Spearman's rank correlation test has been applied to Concept Laser M2 builds in which the process parameters were varied between different sample components. When comparing the programmed local energy density to the DSCNN's *soot* and *debris* classifications (Figure 18), the correlation coefficient is 0.65 with a p-value of 0.0001, indicating a moderate correlation and a very strong reason to accept the correlation. In plain language, this indicates that an increased local energy input can generate abnormal levels of spatter and disrupt the surrounding powder bed. Therefore, one may infer that if *soot* and *debris* are detected during a build fused with nominal process parameters, then unintended off-nominal melting may be occurring.

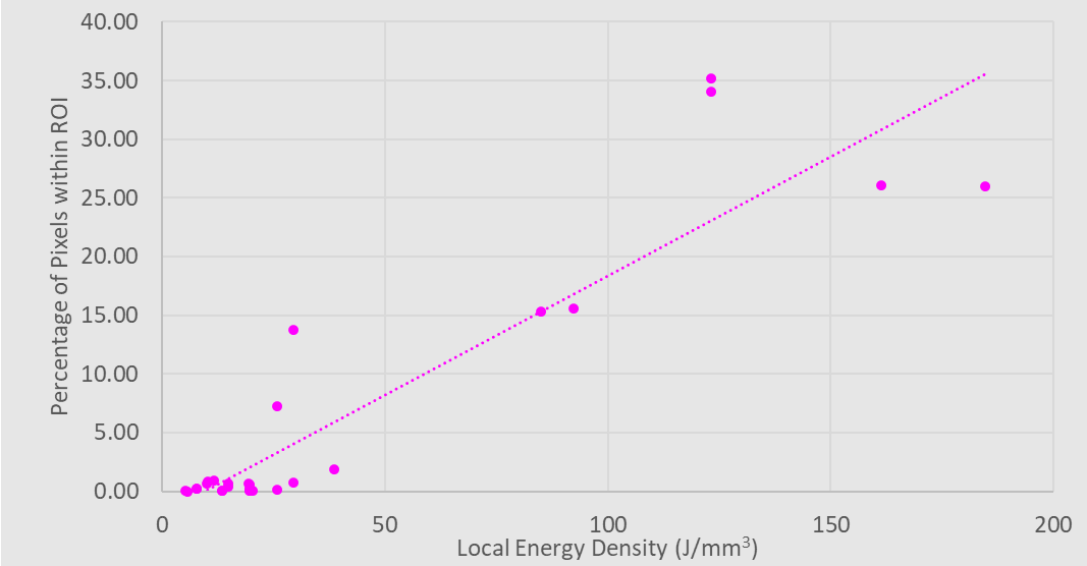

Figure 18: Dynamic segmentation convolutional neural network detections of *soot* and *debris* near a given sample component plotted against the programmed energy density of the sample component.
(ROI = region of interest.)

3.3 UNSUPERVISED MACHINE LEARNING

The sample components from the Concept Laser M2 parameter studies were cross-sectioned ex situ and imaged with an optical microscope. Thresholding techniques implemented in ImageJ were used to quantify the amount and circularity of the 2D porosity present in each sample. Spearman's rank correlation test was unable to identify any statistically significant correlations between the porosity and the in situ data, so an unsupervised ML technique known as t-distributed stochastic neighbor embedding (t-SNE) was implemented. For this test, each sample component was represented by a high-dimensional set of features generated by the DSCNN from the in situ visible-light imaging data. The tSNE algorithm attempts to cluster samples with similar features while separating samples with different features. Figure 19 shows a clustering of the data where each dot represents one sample component and the color of the dot indicates the amount of circular porosity found in the ex situ cross section.

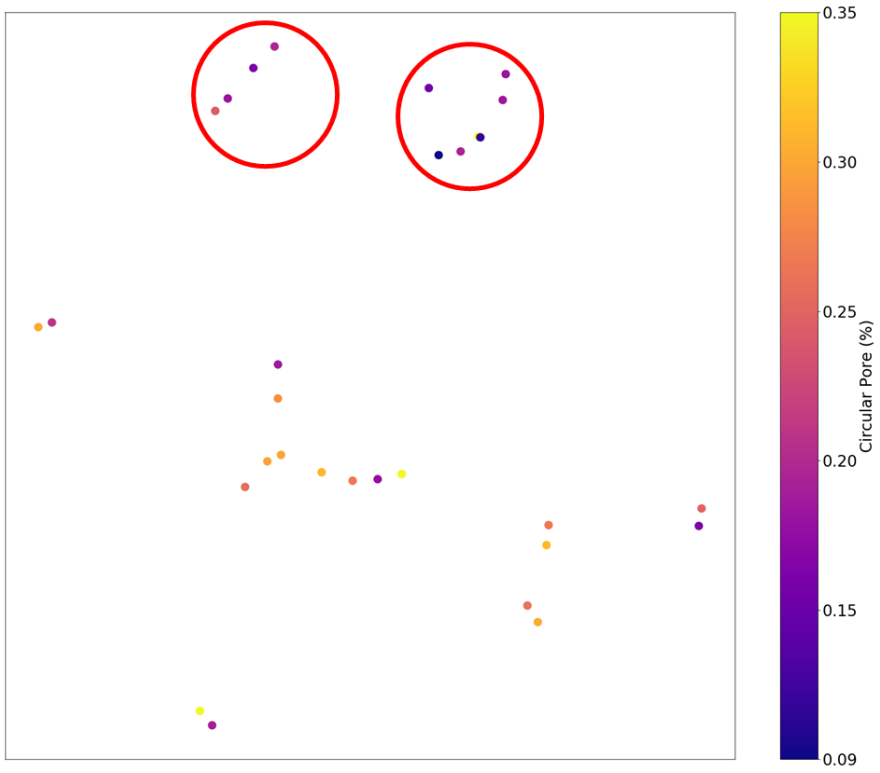

Figure 19: Clustering of samples from a process parameter study using t-distributed stochastic neighbor embedding. Each dot is a sample represented by a set of features extracted by the dynamic segmentation convolutional neural network technique. The color of each dot represents the porosity level within the corresponding sample.

It is important to note that the above plot is completely dimensionless and the spacings between the dots are highly nonlinear. Nonetheless, the samples with the lowest levels of porosity are distinguishable by their in situ features, forming two distinct clusters as highlighted by the red circles. These correlations are preliminary and additional work is required to validate the robustness of this approach (for example, there is a high porosity sample located in one of the clusters of primarily low porosity samples); however, the results are promising and motivating several of the future approaches being considered by the TCR team.

3.4 REGISTRATION WITH WHITE LIGHT SCANS

Ten tubes from the build shown in Figure 15 were subjected to a burst test. Once the test was completed, one of these tubes was scanned using a structured-light measurement system to generate a 3D mesh of its envelop. The scan was then compared to the in situ data measurements to highlight the correlation between the detected defect in situ and the failure point location. The results are presented in Figure 20. First a distance measurement between the mesh of the CAD model and the in situ mesh was used to highlight the visible deviation described in Sect. 3.1. In this example, a short distance or perfect match is represented by the color green and significant deviation appears in red. We then placed the mesh of the scan next to the deviation map to show that the location of the burst corresponds to the location of the detected defect.

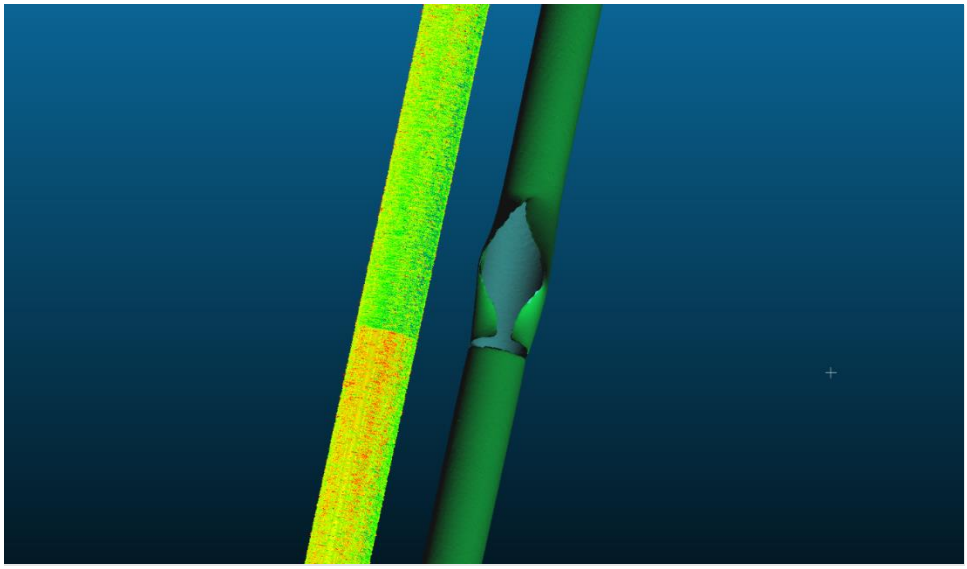

Figure 20: Comparison of detection of defect in situ and the location of the failure point in the physical object.

3.5 IN SITU AND EX SITU TOPOLOGICAL ACCURACY WITH STRUCTURED-LIGHT SCANNING

In additive manufacturing (AM), a critical factor in part performance is the raw morphological accuracy of the printed part. For DED systems, this can be evaluated in situ using DIC to construct a 3D scan of the observable outer surfaces of the part. These scans can be compared to the ex situ technique of structured-light scanning (SLS), available at the ORNL Manufacturing Demonstration Facility through partnership with Zeiss and the COMET 6 SLS system. A comparison of the two techniques is shown in Figure 21.

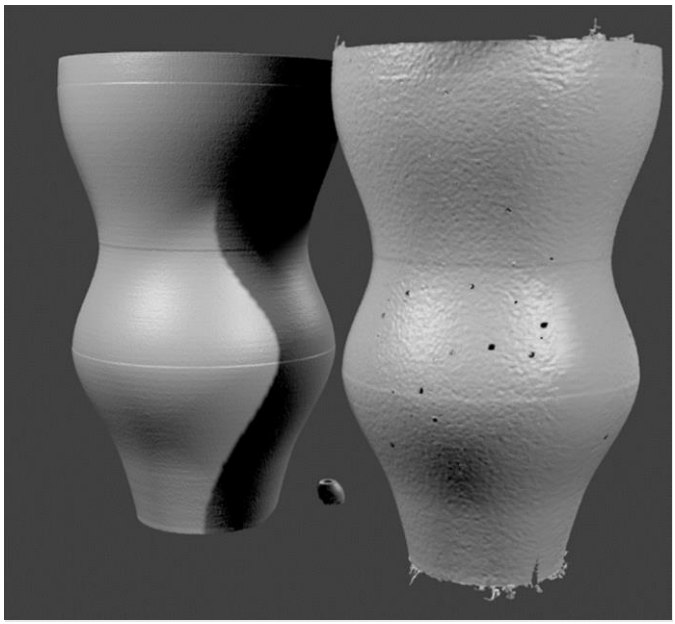

Figure 21: Comparison of ex situ structured-light scanning (left) to in situ digital image correlation (right).

DIC obtains a lower resolution as it depends on the existence of surface features for correlation; however, it also obtains strain information and processes the entire image in one camera exposure (as opposed to dozens), allowing it to capture data at higher speeds and free from motion blur.

3.6 SURFACE ROUGHNESS CORRELATION

In AM, roughness is commonly generated by (a) layer-by-layer "scalloping" of the sides of the bead due to surface tension and (b) welded-on powder particles that did not melt completely. With high-resolution cameras installed off-axis in non-powder-bed technologies, both forms of surface roughness can be estimated directly based on the variation in light signal intensity.

Measuring surface roughness is important not only for determining the functionality of parts but also for tracking changing conditions in the melt pool. Figure 22 shows results for measuring a printed cylinder with the in situ camera array, which showed variable roughness characteristics from the bottom of the print to the top. This was confirmed with confocal microscopy, showing a transition from a higher degree of scalloping roughness on a band in the middle to a finer, more controlled melt pool size concurrent with more welded powder particles. This regime change did not occur from any external parameter alterations, but instead was likely due to a buildup of heat—common in small components due to the high rate of return (with respect to the laser head) and limited inter-bead cooling time.

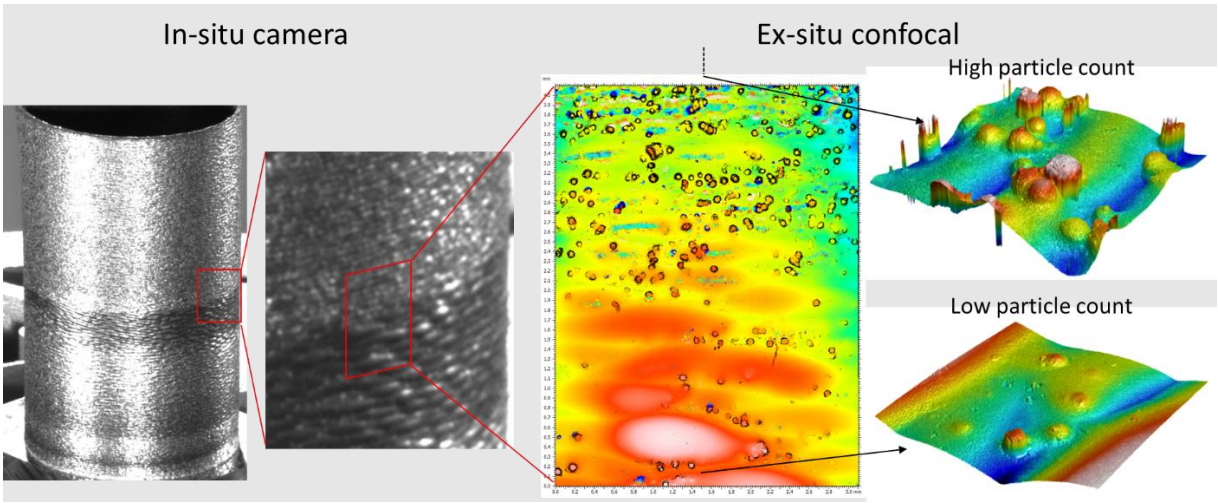

Figure 22: Comparison of in situ high resolution imaging system (left) and ex situ confocal microscopy measurements (right). In both, surface roughness features can be identified, highlighting a process regime change due to thermal buildup that can be identified from the number of powder particles welded to the surface.

Additionally, measuring surface roughness in situ is a necessary step toward obtaining temperature measurements as it effects the emissivity nonuniformly. Extracting a projected 3D map of roughness will make it possible to locally correct the infrared camera signal for more accurate temperature readings in future work. Figure 23 shows an example of the nonuniformity of the IR signal due to surface roughness.

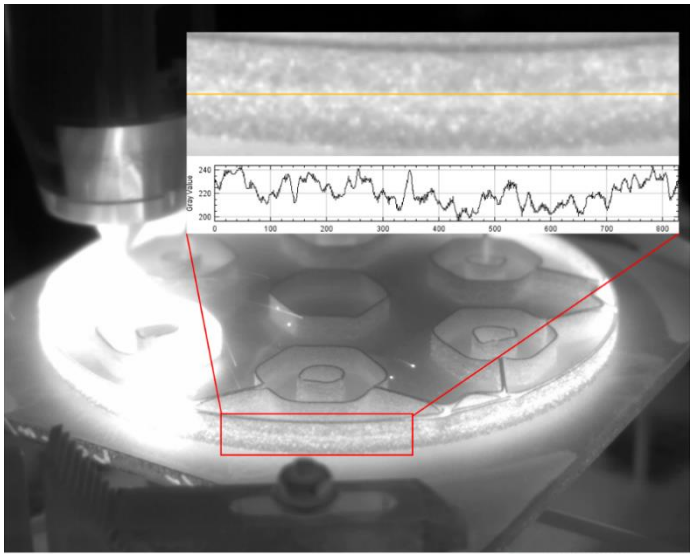

Figure 23: Infrared signal intensity variation due to surface roughness. In an apparently isothermal heated thin wall, the signal varies by up to 20% from local variation in emissivity.

4. CONCLUSION

The program has demonstrated via examples that the integration of sensing modalities combined with advanced data analytics techniques provides a viable alternative to expensive testing campaigns to certify components. The focus was mainly on detecting surface and geometrical defects. As this work progresses, a focus on subsurface defect detection will be required.